[20]K. A. Muller, in *Paramagnetic Resonance*, edited by W. Low (Academic, New York, 1963), Vol. I.
[21]A. W. Hornig, R. C. Rempel, and H. E. Weaver, J. Phys. Chem. Solids 10, 1 (1959).
[22]V. G. Bhide and H. C. Bhasin, Phys. Rev. 159, 586 (1967).
[23]D. J. A. Gainon, Phys. Rev. 134, A1300 (1964).
[24]E. Simanek and Z. Sroubek, Phys. Rev. 163, 275 (1967).
[25]G. K. Wertheim, D. N. E. Buchman, and H. J. Guggenheim, Phys. Rev. B 2, 1392 (1970).
[26]R. V. Pound, G. B. Benedek, and R. Drever, Phys. Rev. Letters I, 405 (1961).
[27]D. N. Pipkorn, C. K. Edge, P. Debrunner, G. Depasquali, H. G. Drickmer, and H. Fraunfelder, Phys. Rev. 135, A1604 (1964); Ref. 38, p. 171.
[28]J. Danon, Intern. At. Energy Agency Tech. Rept. Ser. 50, 89 (1966).
[29]L. R. Walker, G. K. Wertheim, and V. Jaccarino, Phys. Rev. Letters 6, 98 (1961).
[30]R. S. Preston, S. S. Hanna, and J. Heberle, Phys. Rev. 128, 2207 (1962).
[31]T. A. Kovats and J. C. Walker, Phys. Rev. 181, 610 (1969).
[32]R. M. Sternheimer, Phys. Rev. 130, 1423 (1963).
[33]R. Ingalls, Phys. Rev. 133, A787 (1964).
[34]M. R. Haas and J. C. Glass (unpublished).
[35]Yu. Venevtsev *et al.*, Kristallografiya 3, 473 (1958); 4, 255 (1959).
[36]R. R. Hewitt, Phys. Rev. 121, 45 (1961).
[37]S. J. Triebwasser, J. Phys. Chem. Solids 3, 53 (1957).
[38]J. Danon, *Chemical Applications of Mössbauer Spectroscopy*, edited by V. I. Goldanskii and R. H. Herber (Academic, New York, 1968), p. 173.
[39]W. J. Merz, Phys. Rev. 76, 1221 (1949).
[40]For an excellent discussion see Ref. 1, pp. 121, 122, and 145–147.
[41]W. N. Lawless, Phys. Rev. 138, A1751 (1965).
[42]W. Cochran, Phys. Rev. Letters 3, 412 (1959); Advan. Phys. 9, 387 (1960); 10, 401 (1961).
[43]P. W. Anderson, Fizika Dielectrikov AN. SSSR, 290 (1960).
[44]G. K. Wertheim, *Mössbauer Effect: Principles and Applications* (Academic, New York, 1964).
[45]C. Muzikar, J. V. Janovec, and V. Dvorak, Phys. Status Solidi 3, K9 (1963).
[46]See, for example, references given in G. Shirane, J. P. Axe, and J. Harada, Phys. Rev. B 2, 3651 (1970); Kensuke Tani, J. Phys. Soc. Japan 26, 93 (1969).
[47]E. Fatuzzo and W. J. Merz, in *Selected Topics in Solid State Physics*, edited by E. P. Wohlfarth (North-Holland, Amsterdam, 1967), Vol. VII.
[48]C. H. Perry, B. N. Khanna, and G. Rupprecht, Phys. Rev. 135, A408 (1964).

PHYSICAL REVIEW B VOLUME 5, NUMBER 9 1 MAY 1972

Electron-Nuclear-Double-Resonance and Electron-Spin-Resonance Evidence for a Fe^{3+} (K^+ Vacancy) Center in Iron-Doped $KZnF_3$

J. J. Krebs and R. K. Jeck*†
Naval Research Laboratory, Washington, D. C. 20390
(Received 3 January 1972)

Crystals of $KZnF_3$ doped with ≥ 0.05-at.% iron exhibit Fe^{3+} electron-spin-resonance (ESR) and electron-nuclear-double-resonance (ENDOR) spectra which indicate the existence of a charge compensator along a ⟨111⟩ direction. This is over and above the cubic spectrum observed at lower doping levels. The ESR spin-Hamiltonian parameters of the compensated center at 77 °K are $a=+49.7(4)$, $D=+107.9(3)$, and $F=-2.7(4)$ (in units of 10^{-4} cm^{-1}) and $g=2.0029(3)$. The angular ENDOR data for the two sets of three nearest-neighbor fluorines were analyzed to determine the local distortion in some detail. The results are in good accord with a model which assumes that one of the eight nearest-neighbor K^+ ions surrounding the Fe^{3+} is absent.

INTRODUCTION

The transferred hyperfine interactions of the transition-metal ions Mn^{2+}, Fe^{3+}, Co^{2+}, and Ni^{2+} located in the cubic Zn^{2+} sites in the perovskite fluoride $KZnF_3$ have recently been investigated.[1] During the course of this work, electron-spin-resonance (ESR) spectra characterized by maximum splitting for $\vec{H} \| \langle 111 \rangle$ were found in iron-doped $KZnF_3$ crystals and these same samples exhibited ^{19}F electron-nuclear-double-resonance (ENDOR) lines which were clearly not associated with Fe^{3+} in cubic sites. In this paper, we report a thorough-going ESR/ENDOR investigation of these spectra and their source—designated as the Fe-⟨111⟩ center. The characteristics of this center are in substantial agreement with a model involving a nearest-neighbor (nn) K^+ vacancy which locally charge compensates the Fe^{3+} ion. The experiment serves as an excellent example of the power of the ENDOR technique in obtaining detailed information about transition-metal ions in sites lacking local stoichiometry. Such information is, in large measure, unattainable from the ESR spectra of these centers.

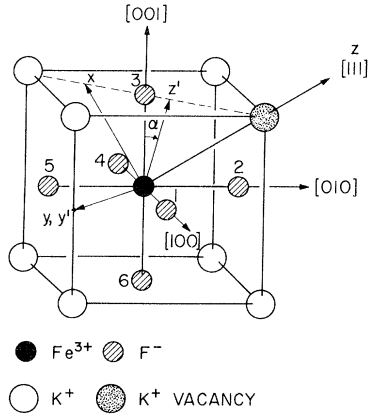

FIG. 1. Fe^{3+}-substituted unit cell of $KZnF_3$ showing the probable location of the charge compensator, viz., a nn K^+ vacancy. The primed coordinate system indicates the principal axes of the superhyperfine (shf) interaction for F^- ion 3, while the unprimed coordinates are a consistent choice for the principal axes of the trigonal crystal field.

Fe-⟨111⟩ Center—A Phenomenological Model

In Fig. 1 we indicate the unit cell[2] of $KZnF_3$ with the central Zn^{2+} replaced by a Fe^{3+} ion. Our experiments show that at sufficiently low Fe^{3+} concentrations ($\lesssim$100 ppm) almost all the Fe^{3+} sites retain O_h point symmetry, implying that any local distortions are purely radial in character. The spin Hamiltonian associated with such a Fe^{3+} ion is then given by[3,4]

$$\mathcal{H}_{\text{cubic}} = g\mu_B \vec{H}\cdot\vec{S} + (a/180)(20\sqrt{2}\,O_4^3 - O_4^0) + \sum_i (\vec{S}\cdot\vec{A}_i\cdot\vec{I}_i - g_n\mu_N\vec{H}\cdot\vec{I}_i), \quad (1)$$

where a threefold axis has been chosen as the reference axis for the cubic crystal field term (in anticipation of the following) and the sum extends over the six equivalent nearest-neighbor fluorines.

When the concentration of Fe^{3+} ions increases, the likelihood of local charge compensation becomes greater with the concomitant appearance of Fe^{3+} ions in distorted sites. The gross features of the Fe-⟨111⟩ spectrum indicate that there is a charge compensator in a ⟨111⟩-type direction in the neighborhood of this center and hence the spin Hamiltonian takes the form

$$\mathcal{H}_{\langle 111\rangle} = g\mu_B\vec{H}\cdot\vec{S} + \tfrac{1}{3}DO_2^0 + \tfrac{1}{9}\sqrt{2}\,aO_4^3 + \tfrac{1}{180}(F-a)O_4^0 + \sum_i (\vec{S}\cdot\vec{A}_i\cdot\vec{I}_i - g_n\mu_N\vec{H}\cdot\vec{I}_i)\ , \quad (2)$$

where the crystal field z axis has been chosen along the ⟨111⟩ distortion and the second- and fourth-order crystal field parameters D and F are consistent with the lowered symmetry (C_{3v}). Furthermore, we expect the other spin-Hamiltonian parameters g, a, and $\vec{A}_i$ to be altered somewhat from their value in the cubic case, although experiment showed that the g tensor remains isotropic to within experimental error as Eq. (2) implies. The presence of a charge compensator along the [111] axis of a particular Fe^{3+} ion is indicated in Fig. 1 by the stippled K^+ symbol. The x, y, and z crystal field axes for such a center are taken along $[\bar{1}\bar{1}2]$, $[1\bar{1}0]$, and [111], respectively. This choice eliminates the need for any nonreal crystal field parameters.[4] It is important to have a specific choice for these axes since the fluorine hyperfine interactions, which have their own set of principal axes ($x'y'z'$), must be expressed in the crystal field axis system for calculation. When the C_{3v} symmetry of the center is taken into account, the mirror plane formed by the Fe^{3+}, the charge compensator, and a given F^- ion is the only symmetry element possessed by the nn-F^- hyperfine interaction. If we consider the F^- labeled 3 in Fig. 1, then $[1\bar{1}0]$ is the normal to this plane and is taken as the y' axis. The z' axis is that principal axis in $(1\bar{1}0)$ closest to the undistorted ligand direction with the angle α defined as shown. The third principal hyperfine axis x' (not shown in Fig. 1) completes the right-handed set. Note that α is an approximate measure of the angular rotation of the Fe^{3+}-F^- bond direction induced by the charge compensator.

Since the charge compensator defines a specific ⟨111⟩ *direction* with respect to the Fe^{3+} ion, one can expect that the three nn fluorines closest to the compensator will be distinct from the three which are farther away. Thus the hyperfine tensor ($\vec{A}_f$) for the "front" fluorines labeled 1–3 in Fig. 1 will be distinguishable from that ($\vec{A}_b$) of the "back" fluorines labeled 4–6.

EXPERIMENTAL RESULTS

Samples and Techniques

The single crystals of $KZnF_3$ used were grown from the melt in our laboratory. After extraction from the boules, the crystals were x-ray aligned and cut to produce samples roughly 2–3 mm on a side, having a nominal iron concentration of 0.05–0.08 at.%. The samples were mounted so the magnetic field $\vec{H}$ could be rotated in {100} or {110} planes. The ESR/ENDOR data were obtained using a 16-GHz spectrometer described elsewhere[1] and all the ENDOR work was done at liquid-helium temperature (LHeT).

ESR Results

If $\vec{H}$ is rotated in the $(1\bar{1}0)$ plane, the ESR spectrum of the Fe-⟨111⟩ centers has its maximum total spread when $\vec{H}$ is parallel to [111] or $[11\bar{1}]$, and the spectrum observed under these conditions is shown in Fig. 2. For $\vec{H}\parallel[111]$, we observe primar-

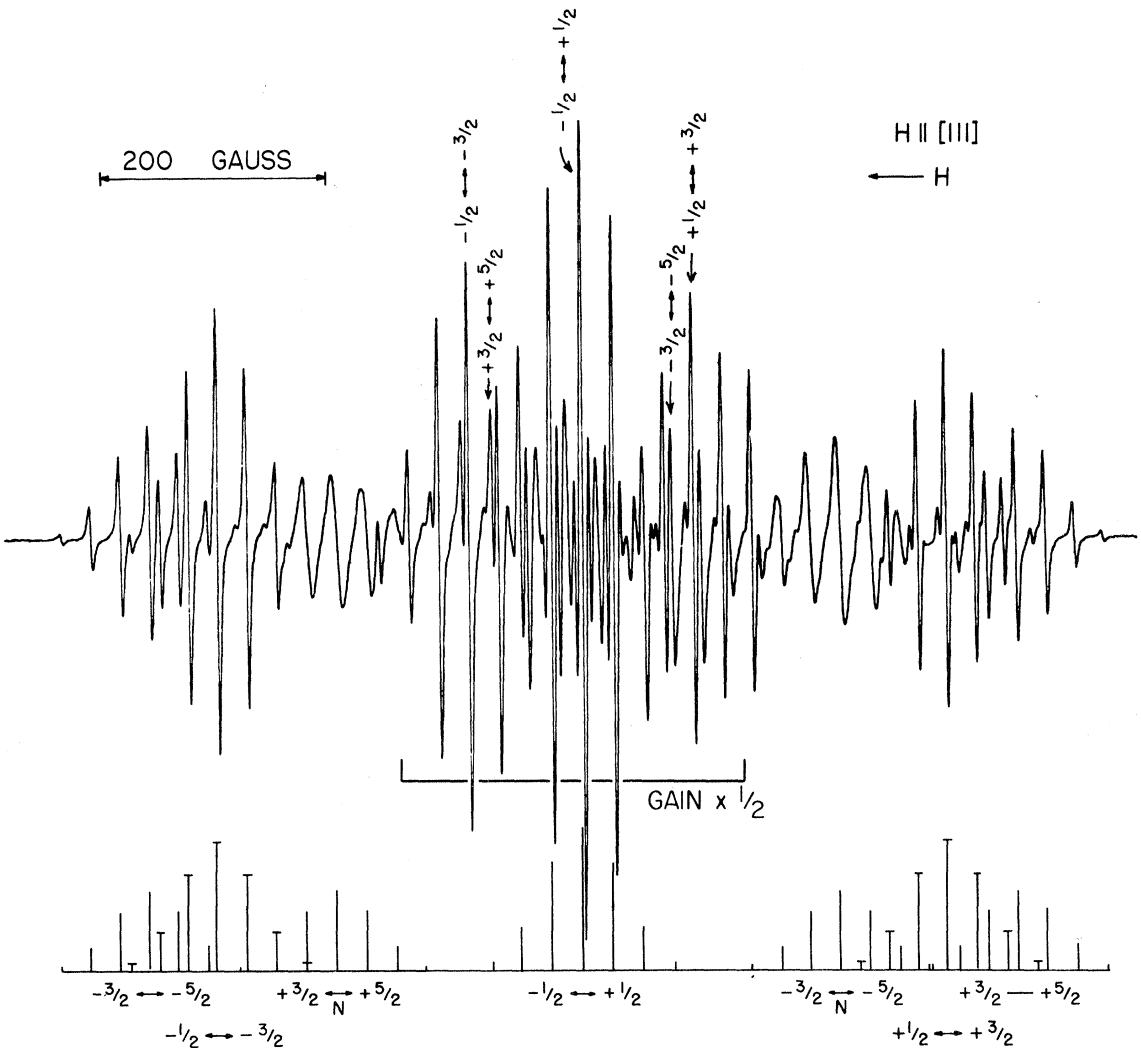

FIG. 2. Observed Fe^{3+} ESR spectrum in $KZnF_3$ with $\vec{H} \parallel [111]$ at 77 °K. The stick diagram marks the position and expected intensity of the lines associated with the Fe-⟨111⟩ center. The transitions labeled N arise from centers whose distortions are along $[11\bar{1}]$, $[1\bar{1}1]$, or $[\bar{1}11]$, while the outer transitions arise from [111] distorted centers. The central line of each fine-structure set of the cubic Fe^{3+} spectrum is marked with an arrow.

ily those Fe-⟨111⟩ centers whose charge compensators are along [111] (or $[\bar{1}\bar{1}\bar{1}]$) and the assignment of the transitions in the outer regions of the spectrum in Fig. 2 are shown. They are the $M = \pm\frac{3}{2} \leftrightarrow \pm\frac{5}{2}$ and $\pm\frac{1}{2} \leftrightarrow \pm\frac{3}{2}$ electronic transitions which are split into multiplets by the superhyperfine (shf) interactions with the nn fluorine ligands. The corresponding $\frac{1}{2} \leftrightarrow -\frac{1}{2}$ set is hidden under the cubic Fe^{3+} spectrum in the central region of the figure. For clarity, the center lines of the various cubic Fe^{3+} hyperfine sets are also indicated in Fig. 2.

For this field orientation, the remaining six types of Fe-⟨111⟩ centers are all magnetically equivalent and $\vec{H}$ makes an angle of 70.5° (or 109.5°) with their distortion directions. They give rise to the hyperfine sets labeled N ($\pm\frac{3}{2} \leftrightarrow \pm\frac{5}{2}$) in the stick diagram of Fig. 2. The corresponding $\pm\frac{1}{2} \leftrightarrow \pm\frac{3}{2}$ and $\frac{1}{2} \leftrightarrow -\frac{1}{2}$ sets are buried in the central region of the spectrum. When the greater width of the N spectrum lines is taken into account, the integrated intensity is in reasonable accord with expectation (i.e., roughly three times the Fe-[111] intensity). This width is apparently due to a small sample misorientation which removes the equivalence of the Fe-⟨111⟩ centers whose axes are not parallel to $\vec{H}$. Note that the Fe-[111] hyperfine sets have very nearly the 1:6:15:20:15:6:1 intensity ratio expected for six equivalent fluorines. This shows that $\overleftrightarrow{A}_f$ and $\overleftrightarrow{A}_b$ are not greatly different.

For $\vec{H} \parallel [100]$, the Fe-⟨111⟩ spectrum collapses

TABLE I. Experimental spin-Hamiltonian parameters for the Fe-⟨111⟩ center in $KZnF_3$ (units of 10^{-4} cm^{-1}, except g). The error in the last digit is indicated.

	300°K	77°K
g	...	2.0029(3)
D	103.4	107.9(3)
a	45.6	49.7(4)
F	−3.9	−2.7(4)
a_{cubic}	52.7[a]	56.9(2)[a]

[a]See Ref. 1.

onto the cubic spectrum and the only discernible hyperfine set is the $\frac{1}{2} \leftrightarrow -\frac{1}{2}$ which is some 6 G upfield from the corresponding cubic set. This collapse is in accord with expectation for this orientation since $\vec{H}$ makes an angle θ_i with all ⟨111⟩ such that $3\cos^2\theta_i - 1 = 0$ and the first-order effect of D vanishes. The 6-G displacement of the $\frac{1}{2} \leftrightarrow -\frac{1}{2}$ set is in quantitative agreement with the second-order effects calculated from the spin-Hamiltonian parameters. For all other orientations of $\vec{H}$ which deviate significantly from $\vec{H} \parallel \langle 111 \rangle$ including $\vec{H} \parallel \langle 110 \rangle$ the spectrum is too complex to allow easy separation of the various components.

The spin-Hamiltonian parameters derived from the observed spectra are shown in Table I. For comparison, we also list the value of a_{cubic} for the undistorted site. The more accurate liquid-nitrogen temperature (LNT) parameters were obtained using a computerized least-squares fit[5] to the angular-dependent data near $\vec{H} \parallel [111]$. The absolute signs of the parameters were determined from the relative intensities of the various fine-structure hyperfine sets at 4.2°K. In the above analysis the shf interaction with the ligands was ignored. This approximation does not have a significant effect on the quoted ESR parameters.

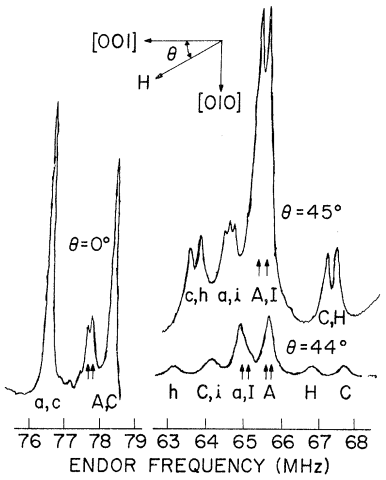

FIG. 3. Portions of the observed nn fluorine ENDOR spectrum corresponding to $\langle S_z \rangle = -\frac{1}{2}$ at 4.2°K. The arrows mark the positions of the doublets arising from Fe^{3+} in cubic sites, while the upper- and lower-case letters refer to fluorines associated with various Fe-⟨111⟩ centers (see Table III). For $\theta = 45°$ ($\vec{H} \parallel [110]$), the equivalence of pairs of fluorines belonging to the same center leads to a doublet splitting.

ENDOR Results

In samples containing the Fe-⟨111⟩ center, the ENDOR spectrum for nn fluorines exhibits lines corresponding to this center as well as those previously found for the cubic Fe^{3+} center.[1] An example of some of the data obtained is shown in Fig. 3 for several magnetic field directions in (100). The cubic ENDOR transitions are marked with arrows, while the Fe-⟨111⟩ ENDOR lines are labeled according to a scheme which will be explained shortly.

The angular dependence of the Fe-⟨111⟩ ENDOR lines corresponding to an electron magnetic quantum number $M = -\frac{1}{2}$ was measured for $\vec{H}$ rotating in both (100) and $(1\bar{1}0)$ at LHeT. The (100) data, which are the most complete, are shown in Fig. 4. The solid curves represent theoretical fits using the parameters

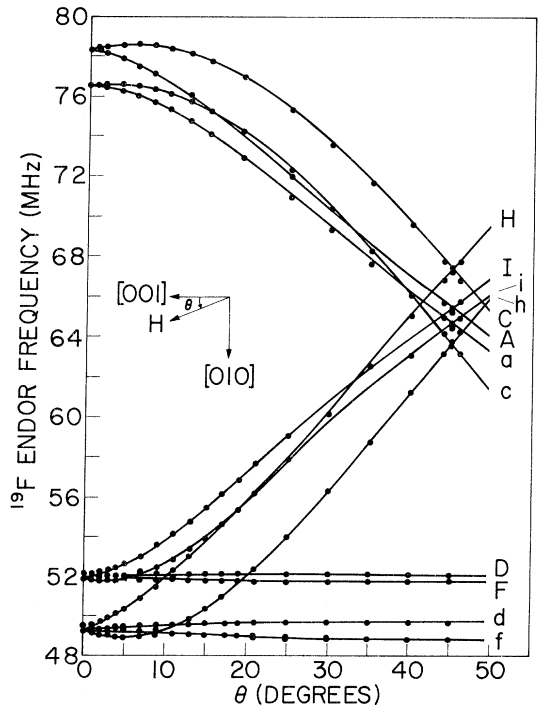

FIG. 4. Angular dependence of the nn-fluorine ENDOR spectrum corresponding to $\langle S_z \rangle = -\frac{1}{2}$ for $\vec{H}$ in (100). The data points were measured at 4.2°K and the solid lines are computer-generated curves using the spin-Hamiltonian parameters listed in Tables I and II. The labeling scheme for the various curves is explained in Table III.

TABLE II. Experimental nn fluorine hyperfine parameters[a] for the Fe-⟨111⟩ center in $KZnF_3$ at LHeT (units of MHz).

	Set I (front fluorine)	Set II (back fluorine)
$A_{x'}$	54.26	48.78
$A_{y'}$	54.30	48.84
$A_{z'}$	109.52	105.36
α	−2.8°	+1.1°

[a]Typical errors are ±0.1 MHz for $A_{i'}$ and ±0.3° for α.

shown in Tables I and II. As is obvious from the data of Fig. 4, there are two sets of shf parameters which are to be associated with the front and back nn fluorines. The assignment will be discussed later.

The method used to fit the ENDOR data of Fig. 4 is worthy of mention. It involved an exact computer diagonalization of the Hamiltonian to obtain the ENDOR frequencies. Each fluorine ion nn to a given Fe-⟨111⟩ center was treated independently, that is, the mutual interaction of these fluorines was neglected. The hyperfine interaction of a given F^- can be written in its own principal coordinate system (see Fig. 1) as

$$\mathcal{H}_{\rm hf} = \sum_i A_i S_i I_i, \quad i = x', y', z'. \tag{3}$$

Since the primed axes do not coincide with the crystal field axes, the hyperfine tensor is transformed into the latter system by a rotation of $[\cos^{-1}(1/\sqrt{3})] - \alpha$ about the y' axis. Now, for a given field direction, there are several F^--Fe-⟨111⟩ combinations which will yield distinguishable ENDOR lines. For convenience, the distinguishable sets for $\vec{H}$ rotating in (100) or (1$\bar{1}$0) are listed in Table III. The designations found there correspond to those used in Figs. 3 and 4 to label the observed ENDOR transitions. It should be emphasized, however, that there is an inherent ambiguity in the assignments since one can make a one-to-one exchange of the corresponding upper- and lower-case letters in the absence of considerations distinct from the raw data.

Since each case listed in Table III has its own local coordinate system, the electronic and nuclear Zeeman terms were expressed in each of these systems by finding the components of $\vec{H}$ in them. It is possible to do this systematically from rather simple geometric considerations. We then have a number of 12×12 ($S=\frac{5}{2}$, $I=\frac{1}{2}$) eigenvalue matrices to solve numerically to obtain the ENDOR frequencies for various orientations of $\vec{H}$. In general, the Zeeman matrix elements will be complex since the (dominant) electronic Zeeman term is not diagonal in the local coordinate systems. Such a matrix is poorly suited to perturbation calculations but offers considerable simplicity for computer calculation of the eigenvalues.

Since all the principal hyperfine values of both the front and back fluorines can be found by rotating $\vec{H}$ in a (110) plane, such data were used to obtain an estimate of these values via perturbation formulas which ignored crystal field effects. These estimates were in turn refined by comparing the computer-calculated ENDOR frequencies with experiment and iterating. The data for $\vec{H}$ in (100) (Fig. 4) allow one to sort out which hyperfine constants belong to the same set. As can be seen, the final choice is consistent and gives an excellent fit to the data. Although as Fig. 4 shows, the maxima and minima of the ENDOR frequencies occur several degrees away from the cube-edge direction for $\vec{H}$ in (100), most of this angular deviation is due to the D term in the spin Hamiltonian rather than the effect of α. This was established by computer calculation. Classically stated, the D term makes it energetically favorable for the Fe^{3+} moment to lie in the plane normal to the distortion axis and hence $\vec{S}$ is not parallel to $\vec{H}$ unless $\vec{H}$ is in or normal to this plane.

The origin of the doublet lines shown in Fig. 3 for $\vec{H}\parallel[110]$ ($\theta = 45°$) and those evident near 49 and 52 MHz in Fig. 4 for $\vec{H}\parallel[100]$ lies in the equivalence of pairs of F^- ions belonging to the same Fe-⟨111⟩ center for these special orientations. Under these conditions, the analysis used above is no longer adequate. Rather, there is a spin-spin interaction between the equivalent nuclei which lifts the degeneracy and gives rise to the observed ENDOR doublets.[6] Note that when the field is misoriented as little as 1° from the symmetry axis (Fig. 3, $\theta = 44°$), the doublets are no longer clearly resolved since the equivalence is broken. Our neglect of this effect in the above ENDOR fitting procedure does

TABLE III. Classification of representative F^- charge-compensator combinations.[a]

Front case	Reference F^- ion[b]	Back case	Reference F^- ion[b]	Associated charge compensator direction
A	3	*a*	6	[111]
B	6	*b*	3	[11$\bar{1}$]
C	3	*c*	6	[1$\bar{1}$1]
D	1	*d*	4	[111]
E	1	*e*	4	[11$\bar{1}$]
F	1	*f*	4	[1$\bar{1}$1]
G	1	*g*	4	[1$\bar{1}\bar{1}$]
H	5	*h*	2	[1$\bar{1}$1]
I	5	*i*	2	[1$\bar{1}\bar{1}$]

[a] The cases listed provide distinct ENDOR spectra for $\vec{H}$ rotating in (100) or (1$\bar{1}$0).

[b] See Fig. 1 for numbering scheme.

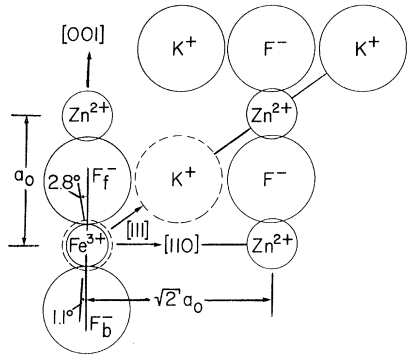

FIG. 5. Schematic representation of the $(1\bar{1}0)$ plane in $KZnF_3$ in the vicinity of a Fe-⟨111⟩ center. The various ions are scaled according to their known crystal radii.

not significantly affect the hyperfine values determined.

Other Results

In addition to the Fe-⟨111⟩ center results noted above, we find a much weaker set of ESR lines whose angular dependence indicates an axially symmetric center with a ⟨100⟩ orientation. The presence of these lines only in iron-doped samples and the observed superhyperfine splitting suggest that they represent another Fe^{3+} center. Likewise, ENDOR lines which correspond to neither the cubic Fe^{3+} nor the Fe-⟨111⟩ center are found and they are consistent with such an axis of symmetry. Unfortunately, the data at our disposal do not allow an unambiguous identification of the center involved. We suggest, however, that the spectra may be due to a small number of Fe^{3+} ions charge compensated in other ways, e.g., via an O^{2-} replacing a F^- along ⟨100⟩. These centers will not be treated further in this paper.

DISCUSSION

The detailed agreement between the phenomenological charge-compensation model of the Fe-⟨111⟩ center and the experimental results leaves little doubt as to its validity. In the following, we propose a specific crystallographic model of the center and discuss some of the implications of the differences between the Fe-⟨111⟩ center and Fe^{3+} in a cubic site.

K^+-Vacancy Model

Potential models for the Fe-⟨111⟩ center are most easily discussed in terms of Fig. 5 which gives a view of the $(1\bar{1}0)$ plane in the neighborhood of such a center. In this diagram the symbols for the ions are scaled to represent their crystal radii and the positions indicated are those in an undistorted $KZnF_3$ crystal. The distortion angles α_f and α_b are also indicated.

The existence of a charge compensator along [111] requires that one of the K^+ or Zn^{2+} ions in this direction be altered. Furthermore, since the distortion is local, only the nn Zn^{2+} and the nn and next-nearest-neighbor (nnn) K^+ need be considered. The proper alteration in the local charge can be obtained most easily by removing one of the K^+ ions or replacing a Zn^{2+} by a K^+. As Fig. 5 makes clear, however, this latter change can be discounted because of the very poor fit of a K^+ ion in a Zn^{2+} site. If we therefore consider only K^+ vacancies, we see that the Coulomb energy is lowered more by a nn than by a nnn K^+ removal although the energy increase associated with the local lattice distortion would be nearly the same in both cases. Furthermore, if nnn K^+ vacancies were present, one would expect to see nn K^+ vacancies also, in contrast to the unique Fe-⟨111⟩ center found. We conclude therefore that the Fe-⟨111⟩ center is due to a Fe^{3+} ion with a nn K^+ vacancy. Unambiguous proof of this identification could be found if the interaction of the Fe^{3+} with the nn K^+ ions could be detected by ENDOR. Unfortunately, we were not able to do so.

Local Changes Induced by K^+ Vacancy

We now consider the choice of which set of shf constants is to be associated with the front and back F^- ions. First we note that even though symmetry allows the hyperfine tensor to be orthorhombic it has axial symmetry to within experimental error. Under this circumstance, each of the hyperfine tensors can be written in the form

$$A(\gamma) = A_s + A_p(3\cos^2\gamma - 1)\,, \tag{4}$$

where γ is the angle between $\vec{S}$ and the axis of symmetry of the hyperfine tensor. These symmetry axes are rotated away from the bond directions in an undistorted crystal (⟨100⟩) by the angles α_f or α_b. In Table IV we list the values of A_s, Ap, and α for the two hyperfine sets and compare them with the cubic case.

From the model of the Fe-⟨111⟩ center given above we expect that the greatest deviation from the cubic case will be associated with the front fluorines since they are immediately adjacent to the charge compensator. The data in Table IV then lead one to assign set I to the front fluorines and set II to the back. (This is reflected in the labeling in Figs. 3 and 4.) In making this choice, the relative sizes of the value found for α in the two cases are crucial since α represents the most clear-cut change. The experimental values of α thus imply that the front fluorines rotate 2.8° away from the distortion axis while the back fluorines rotate 1.1° toward it.

The signs of the change of A_s from the cubic

TABLE IV. Isotropic and anisotropic nn-fluorine hyperfine parameters for the Fe-⟨111⟩ center and cubic Fe^{3+} in $KZnF_3$ (units of 10^{-4} cm^{-1}). For sets I and II, typical errors are 0.03 and 0.02 for A_s and A_p, respectively.

	Set I (front)	Cubic[a]	Set II (back)
A_s	24.25	23.46	22.57
A_p	6.14	6.29	6.29
α	−2.8°	0	1.1°

[a]See Ref. 1.

case are also in agreement with this assignment for the Fe-⟨111⟩ model. The destruction of the O_h symmetry at the Fe^{3+} site caused by the K^+-vacancy results in different relative displacements of the charge centers of gravity associated with the Fe^{3+} and its front and back F^- ions. The net result is to move the Fe^{3+} closer to the front set and away from the back set. Overlap considerations then lead one to expect an increase in A_s for the front set and a decrease for the back. This expectation is borne out by the experimental results. It is interesting to see that the same qualitative changes in A_s are induced by at least one covalency effect. Thus, the removal of a positive charge (creation of a K^+ vacancy) favors increased minority-spin electron-charge transfer from the front F^- to the Fe^{3+} and decreased transfer from the back F^- even in the absence of any corresponding lattice distortion. However, in the actual distorted center additional covalency changes may override this effect. Finally, we note that the signs of the α values found for the front and back F^- ions are consistent with the type of distortion just described.

We would like to emphasize that it is the high resolution associated with ENDOR which permits the detailed confirmation of the Fe-⟨111⟩ model reflected in the above analysis. Normally, the shf interaction between a transition-metal ion and the nn ligands in perovskite fluorides is large enough that ESR measurements provide sufficient accuracy for purposes of analysis and comparison with overlap and covalency calculations. However, we see that the ENDOR method has particular value when one is examining the small changes in these shf parameters which are induced by local perturbations. Especially in the presence of the ESR spectrum due to cubic Fe^{3+} sites, it would be impossible to determine either the minor (< 4%) changes in A_s and A_p or the small angular rotations of the symmetry axes of the F^- hyperfine tensors associated with the Fe-⟨111⟩ center. However, ENDOR makes it possible to measure these changes easily with quite adequate precision.

ACKNOWLEDGMENTS

The authors wish to thank V. J. Folen and R. A. Becker for the synthesis of the samples used in this work.

*Work performed during the tenure of an NAS-NRC Postdoctoral Research Associateship.

†Present address: Smithsonian Radiation Biology Laboratory, Rockville, Md. 20852.

[1]R. K. Jeck and J. J. Krebs, Phys. Rev. B 5, 1677 (1972).

[2]K. Knox, Acta Cryst. 14, 583 (1961). The space group of $KZnF_3$ is O_h^1.

[3]W. Low, in *Solid State Physics*, edited by F. Seitz and D. Turnbull (Academic, New York, 1960), Suppl. Vol. 2.

[4]M. T. Hutchings, in *Solid State Physics*, edited by F. Seitz and D. Turnbull (Academic, New York, 1965), Vol. 16, pp. 227–72. This reference gives the phase convention necessary to completely specify the O_4^3 crystal field term.

[5]A general ESR fitting program due to H. M. Gladney (Program No. 69, Quantum Chemistry Program Exchange, Indiana University) was modified to handle the trigonal symmetry of the problem.

[6]T. E. Feuchtwang, Phys. Rev. 126, 1628 (1962); L. C. Kravitz and W. W. Piper, *ibid.* 146, 322 (1966).